Quaternary Science Reviews 125 (2015) 91–97

Contents lists available at ScienceDirect

Quaternary Science Reviews

journal homepage: www.elsevier.com/locate/quascirev

Arctic climate response to the termination of the African Humid Period

Francesco Muschitiello [a, b, *], Qiong Zhang [a, c], Hanna S. Sundqvist [a, c], Frazer J. Davies [d], Hans Renssen [d]

[a] Bolin Centre for Climate Research, Stockholm University, Svante Arrhenius väg 8, SE106-91 Stockholm, Sweden
[b] Department of Geological Sciences, Stockholm University, Svante Arrhenius väg 8, SE106-91 Stockholm, Sweden
[c] Department of Physical Geography and Quaternary Geology, Stockholm University, Svante Arrhenius väg 8, SE106-91 Stockholm, Sweden
[d] Department of Earth Sciences, VU University Amsterdam, De Boelelaan 1085-1087, 1081 HV Amsterdam, The Netherlands

ARTICLE INFO

Article history:
Received 22 November 2014
Received in revised form
30 July 2015
Accepted 7 August 2015
Available online 22 August 2015

Keywords:
Mid Holocene
African Humid period
Arctic climate
Atmospheric circulation

ABSTRACT

The Earth's climate response to the rapid vegetation collapse at the termination of the African Humid Period (AHP) (5.5–5.0 kyr BP) is still lacking a comprehensive investigation. Here we discuss the sensitivity of mid-Holocene Arctic climate to changes in albedo brought by a rapid desertification of the Sahara. By comparing a network of surface temperature reconstructions with output from a coupled global climate model, we find that, through a system of land-atmosphere feedbacks, the end of the AHP reduced the atmospheric and oceanic poleward heat transport from tropical to high northern latitudes. This entails a general weakening of the mid-latitude Westerlies, which results in a shift towards cooling over the Arctic and North Atlantic regions, and a change from positive to negative Arctic Oscillation-like conditions. This mechanism would explain the sign of rapid hydro-climatic perturbations recorded in several reconstructions from high northern latitudes at 5.5–5.0 kyr BP, suggesting that these regions are sensitive to changes in Saharan land cover during the present interglacial. This is central in the debate surrounding Arctic climate amplification and future projections for subtropical precipitation changes.

1. Introduction

The Mid Holocene is a critical period of climate change for the present interglacial. This transitional phase is characterised by a change in the boundary conditions of the Earth's climate system when the Laurentide and Eurasian ice-sheets had largely vanished, sea-level rise stabilized, and meltwater fluxes became negligible (Debret et al., 2009). Studies on climate cycle periodicities highlight a prominent global discontinuity of periodic modes at 5.5–5.0 kyr BP, suggesting a variation in the regional interplay between atmosphere, ocean, ice, and vegetation (Wirtz et al., 2010). This shift corresponds to a rapid climate oscillation that marks in several reconstructions the inception of a pervasive climate reversal, representing the transition into the Neoglacial cooling, which encompasses major changes of the dominant hydro-climate regimes (Magny and Haas, 2004) and a substantial reorganization of the North Atlantic circulation pattern (Sorrel et al., 2012). Prime candidates for direct forcing upon this widespread climate shift are a combination of changes in orbital configuration and solar activity minima (Magny and Haas, 2004). However, a comprehensive understanding of the triggering mechanism of the mid-Holocene climate changes remains elusive and owing to difficulties with dating accuracy it is problematic to evaluate precisely the contribution of high versus low latitudes.

An overlooked factor for large-scale amplification of climate change during the Mid Holocene is the rapid desertification of the Sahara that is evident in many proxy records, also known as the termination of the African Humid Period (AHP). In fact, reconstructions from both marine and terrestrial environments (deMenocal et al., 2000; Gasse, 2001; Kuhlmann et al., 2004; McGee et al., 2013; Tierney and deMenocal, 2013; Armitage et al., 2015), together with archaeological evidence (Kuper and Kröpelin, 2006; Manning and Timpson, 2014), suggest that subtropical North Africa underwent a widespread vegetation collapse and desertification of the Saharan region at 5.5–5.0 kyr BP, which took place within a few centuries (Tierney and deMenocal, 2013; Shanahan et al., 2015). The abruptness of the vegetation decline

* Corresponding author. Bolin Centre for Climate Research, Stockholm University, Svante Arrhenius väg 8, SE106-91 Stockholm, Sweden.
E-mail address: francesco.muschitiello@geo.su.se (F. Muschitiello).

http://dx.doi.org/10.1016/j.quascirev.2015.08.012
0277-3791/

can be explained mainly in terms of internal, regional dynamics of the climate system resulting either from a non-linear, biogeophysical feedback of the vegetation to the gradual decrease in orbital monsoonal forcing (Claussen et al., 1999; Zhao et al., 2007), or from an intrinsic threshold behaviour of the subtropical hydrological system (Liu et al., 2006). New evidence indicates that a weakening of the African monsoon system during interglacial periods can occur independently from high-latitude forcing (Gibson and Peterson, 2014). Hence, the Sahara can be considered as a potentially critical component of the Earth's climate system (Patricola and Cook, 2008), which could have produced abrupt large-scale climate change during the Mid Holocene through changes in surface albedo and regional temperatures.

To test the sensitivity of the large-scale climate system to the rapid mid-Holocene change in Saharan vegetation cover, we combined a data set of surface temperature reconstructions and output from state-of-the-art global ocean-atmosphere climate model EC-Earth. Specifically, we used proxy records to estimate temperature anomalies across the transition from a vegetated state of the Sahara into more arid conditions, and compared the proxy data with results from two highly idealized sensitivity experiments representing a green Sahara and a desert Sahara. We emphasize that, given the fragmentary knowledge on the mid-Holocene distribution of vegetation over the Sahara, these simulations are not intended to realistically reproduce changes in the spatial extent of vegetation. Rather, the simulated scenarios are used to explore the mechanisms underlying rapid changes in subtropical land cover and to put the results in the context of the atmosphere-ocean circulation shifts recorded in several high-latitude climate reconstructions at 5.5–5.0 kyr BP.

2. Methods

2.1. Proxy data

Quantitative paleoclimatic reconstructions used for the proxy-model data comparison were systematically selected from a newly published and exhaustive database of Arctic Holocene proxy climate records (Sundqvist et al., 2014). Regrettably, yet there are no quantitative paleoclimatic records from the Sahara. Therefore, a direct comparison between reconstructions and model output data was not possible for this sector. Individual paleoclimate records were critically evaluated prior to inclusion in the database according to the following criteria: *i*) records are located north of 58°N; *ii*) the proxy records have a demonstrated relation with surface temperatures; *iii*) time-series are continuous and include (at minimum) the entire 6.0 to 2.0 kyr BP interval; *iv*) records are resolved at sub-millennial scale; *v*) records are constrained by at least one chronological data point every 3000 years back to 6.0 kyr BP; *vi*) all records and paleoclimate estimates were published in the peer-reviewed literature.

To assess the performance of our simulations, we decided to further circumscribe the number of proxy records by imposing strict chronological and resolution criteria. We narrowed down the selection of the temperature records to reconstructions that presented age sample resolutions higher than 250 years and geochronology accuracy scores higher than 0 as described in Sundqvist et al. (2014). Thus, we identified in total 46 temperature proxy reconstructions. A full list of sites and records used in this study is presented in Supplementary Table S1.

Our goal is to compare the simulated desert and green Sahara conditions with proxy data evidence after and before the mid-Holocene desertification of the Sahara, which occurred at 5.3 ± 0.3 yr BP according to the most accurate chronologies (Garcin et al., 2012). We thus defined two reference periods for which we calculate the temperature change recorded in the proxy records. The two periods were defined as the 1000-years intervals centred on 6.0 kyr and 5.0 kyr BP, respectively. We consider this as a suitable temporal framework for comparison with the simulations, encompassing the transition from a vegetated state of the Sahara into more arid conditions. We are aware that the upper reference interval is relatively too old with respect to the age for termination of the AHP, but this enables us to avoid the influence from negative temperature anomalies associated with the 4.2 kyr BP cold event (e.g. Bond et al., 2001), which might add substantial biases on our calculations. Hence, it should be born in mind that the climate anomalies presented here are a conservative estimate of the climate change at the transition out of the AHP.

It seems prudent to assume that 1000-years time windows should provide a meaningful quantification of climate change between the two periods, minimizing the possible effects from internal high-frequency climate variability. We thus averaged the reconstructed temperature data over the 1000-years windows defined as 6.0 ± 0.5 kyr BP and 5.0 ± 0.5 kyr BP, respectively. However, three proxy series did not extend up to 6.5 kyr BP. We therefore defined a different lower time window for these series, i.e. 5.75 ± 0.25 kyr BP.

All non-annual time-series were linearly interpolated to 10-years resolution before calculating the 1000-years averages. Temperature anomalies between the two reference periods were then estimated subtracting the 1000-years mean at 6.0 kyr BP from the mean at 5.0 kyr BP ($\Delta T_{5kyr-6kyr}$). In addition, we calculated the statistical significance associated with the anomalies using a Bayesian estimation test, which provides a probability distribution over the difference between two sample populations (Kruschke, 2013).

2.2. EC-Earth model description and experiment setup

The global climate model EC-Earth was used to undertake the two sensitivity experiments in the present study. EC-Earth is developed by a consortium of European research institutions, which collaborate in the development of a new Earth System Model (ESM). The goal of EC-Earth is to build a fully coupled Atmosphere-Ocean-Land-Biosphere model usable from seasonal to decadal climate prediction and climate projections (Hazeleger et al., 2010). The atmospheric component of EC-Earth is based on the modelling systems, i.e. Integrated Forecasting System (IFS), which is developed at the European Centre for Medium-Range Weather Forecasts (ECMWF), and the ocean component is based on Nucleus for European Modelling of the Ocean (NEMO) (Madec, 2008), including a sea-ice model LIM3 (Bouillon et al., 2009). The ocean/ice model is coupled to the atmosphere/land model through the OASIS 3 coupler (Valcke, 2006).

A number of model integrations such as historic simulations (e.g. 1850 to 2005 with known climate forcing such as greenhouse gas, volcanic, aerosol etc.) and scenarios of future possible climates taking into account an increased amount of greenhouse gases (e.g., RCP45, RCP85 etc.) have been conducted using EC-Earth version 2.3. These results contribute to the CMIP5 (Climate Model Intercomparison Project Phase 5) experiments, which form an essential part of the IPCC Fifth Assessment Report. An evaluation of EC-Earth for the Arctic shows that the model simulates the 20th century Arctic climate reasonably well (Koenigk et al., 2013). However, sea-ice thickness and extent are overestimated compared to observations and reanalyses. EC-Earth is also used for past climate studies. For instance, the effect of mid-Holocene orbital forcing on summer monsoons is investigated with EC-Earth 2.3 (Bosmans et al., 2011) and results confirm the findings from proxy data on the monsoon behaviour during this period.

In the present study we use the latest version EC-Earth 3.1. The atmospheric model is based on IFS cycle 36r4 with configuration runs at T159 horizontal spectral resolution (roughly 1.125 × 1.125°) and 62 vertical levels. The ocean component is based on version 2 of the NEMO model with a horizontal resolution of nominally 1° and 42 vertical levels. Boundary conditions for both our sensitivity experiments – including orbital forcing and greenhouse gases – were set to mid-Holocene as 6.0 kyr following PMIP protocol. The orbital forcing was internally computed using the method of Berger (1978). Aerosols, solar radiation, vegetation, ice sheets, topography and coastlines were set to pre-industrial conditions. Following the line of thinking of Davies et al. (2015), the vegetation type was set to 100% shrub for an idealized "green Sahara" (GREEN) over the domain 15°W-35°E and 11–33°N and to 100% desert over the same area for an idealized "desert Sahara" (DESERT). The albedo is 0.15 for shrub and 0.4 for desert. The leaf area index was set to 2.6 for shrub and 0 for desert. The details of boundary conditions are listed in Supplementary Table S2. Initial conditions were taken from a 700-years pre-industrial spin-up run and then the model was run for 250 years. The climate reaches a state of quasi-equilibrium after 100 years - this includes a stable North Atlantic meridional overturning circulation (AMOC) with maximum around 22 Sv in both runs. In this study we focus on the equilibrium responses and the changes we analyze are averaged over the last 100 years of the two sensitivity experiments. Since the dynamical vegetation model has not been included in the current EC-Earth version, the albedo effect due to the change of the vegetation type is dominant in surface energy balance. The albedo is thus controlled by changes in surface latent heat flux and sensible heat flux following the variation in leaf area index, including variations in evaporation and transpiration. The change in surface roughness has not been taken into account in our experiments.

3. Results and discussion

3.1. Proxy-model data comparison

During boreal summer, proxy-based temperature records from Arctic latitudes generally show a decrease in $\Delta T_{5kyr-6kyr}$ of the order of ~0.5 °C, with cooling over Greenland, the North Atlantic and Northern Europe, whereas records located in Labrador, Northwest Territories and Alaska indicate warmer climatic conditions of the order of ~0.5 °C (Fig. 1a). By contrast, winter temperature reconstructions show a rather consistent shift towards colder conditions over the entire Arctic-North Atlantic domain with an average decrease of ~1.0 °C (Fig. 1b).

Our simulations show that the change from shrub vegetation to desert results in higher surface albedo over the Sahara, leading to substantially lower North African surface temperatures in experiment DESERT relative to experiment GREEN (Fig. 1). In DESERT Arctic temperatures decrease on average by ~1 °C during summer and ~2 °C during winter compared to GREEN, with the exception of localized positive summer temperature anomalies in Labrador, Northwest Territories, Alaska, and eastern Siberia, where a warming of ~0.5 °C is observed (Fig. 1). The maximum temperature drop is located in the Barents Sea where temperatures decrease as much as ~11 °C during winter owing to enhanced sea-ice formation (Fig. 2)a. The relatively higher rates of sea-ice production in the Nordic Seas results in increased sea-ice drifting along the eastern Greenland Current, with the excess in sea ice ultimately routed into the Labrador Sea. In addition, sea-level pressure (SLP), which responds directly to surface temperature differences, rises from 1 to 2 hPa over the Arctic, the subarctic regions, and the North Atlantic (Fig. 2b).

The simulated high-latitude climate change is an effect of the decrease in surface temperatures over the Sahara. The lowering of North African surface temperatures results in *i*) a weaker equator-to-subtropical temperature gradient (Fig. 3a) – which turns into a weakening of the atmospheric baroclinicity and reduced eddy activity at mid-to-high latitudes – and *ii*) a decrease in the AMOC intensity (Fig. 3b). These processes result in a reduction of the northward meridional atmospheric and oceanic heat transport conveyed to high northern latitudes (Fig. 3c). The seasonal pattern of climate change recorded in the proxy data is in good agreement with results from our DESERT- GREEN simulations, which appear to capture the spatial distribution of $\Delta T_{5kyr-6kyr}$ (Fig. 1). Hence, the regional distribution of temperature change observed in the network of proxy data gives support to the simulated reduction in northward atmospheric-oceanic heat transfer. Moreover, the consistency between model and proxy data over the Northern American continent, where localized positive summer temperature anomalies are observed (Fig. 1a), gives further confidence on the reliability of our model results.

However, despite the general agreement between model and proxy data, the magnitude of the temperature anomalies appears to be overestimated in the model. This could be explained by the idealized nature of the experiments, which by simulating a widespread desertification event over the whole Sahara may not realistically reproduce the actual time-space complexity of the regional hydrological shifts (e.g. Shanahan et al., 2015). On the other hand, the underappreciated temperature change by proxy data may also play a role owing to complications related to the selection of an appropriate time window for calculation of the climate anomaly. This is due to the position of the upper reference period, which might be relatively too old with respect to the actual desertification event, thereby unable to fully capture the climate response to the termination of the AHP in its entirety (see section 2.1).

Nonetheless, it seems more likely that the model tends to overrepresent the pattern of temperature anomalies. In first instance, the regional cold winter bias simulated over the Barents Sea is a recurrent, prominent and fairly robust feature among global climate models (Arzel et al., 2005; Chapman and Walsh, 2007; Koenig et al., 2013). The bias is the result of topographic smoothness, especially over Greenland, which causes reduced downstream cyclogenesis (Chapman and Walsh, 2007). The truncation of the North Atlantic storm track induces positive SLP biases, a substantial over-simulation of the extent of se ice, and hence the surface air temperature biases in the Barents Sea, which can reach up to 6–8 °C when compared with observations (Chapman and Walsh, 2007). The Barents Sea bias is however a localized feature and the large-scale atmospheric circulation response to Sahara desertification is substantiated by a comprehensive suite of sensitivity experiments with an Earth model of intermediate complexity using various combinations of vegetation covers (Davies et al., 2015).

3.2. Shifts in atmospheric circulation and climate change at 5.5–5.0 kyr BP

Bearing in mind that our approach leans on an idealised experimental design, the results presented here suggest that mid-Holocene desertification in the Sahara had likely a critical influence on climate at high northern latitudes. Through a vegetation-atmosphere feedback the meridional temperature gradient between the subtropics and high latitudes is weakened, leading to a reduction of mid-high latitudes eddy activity and oceanic AMOC. This reduction results in a net decrease in atmospheric and oceanic poleward heat transport. We argue that this mechanism could have had an active role on the hydro-climate and hydrographic changes that are often recorded in proxy reconstructions at 5.5–5.0 kyr BP (e.g. Magny and Haas, 2004), and that a strong causal mechanisms

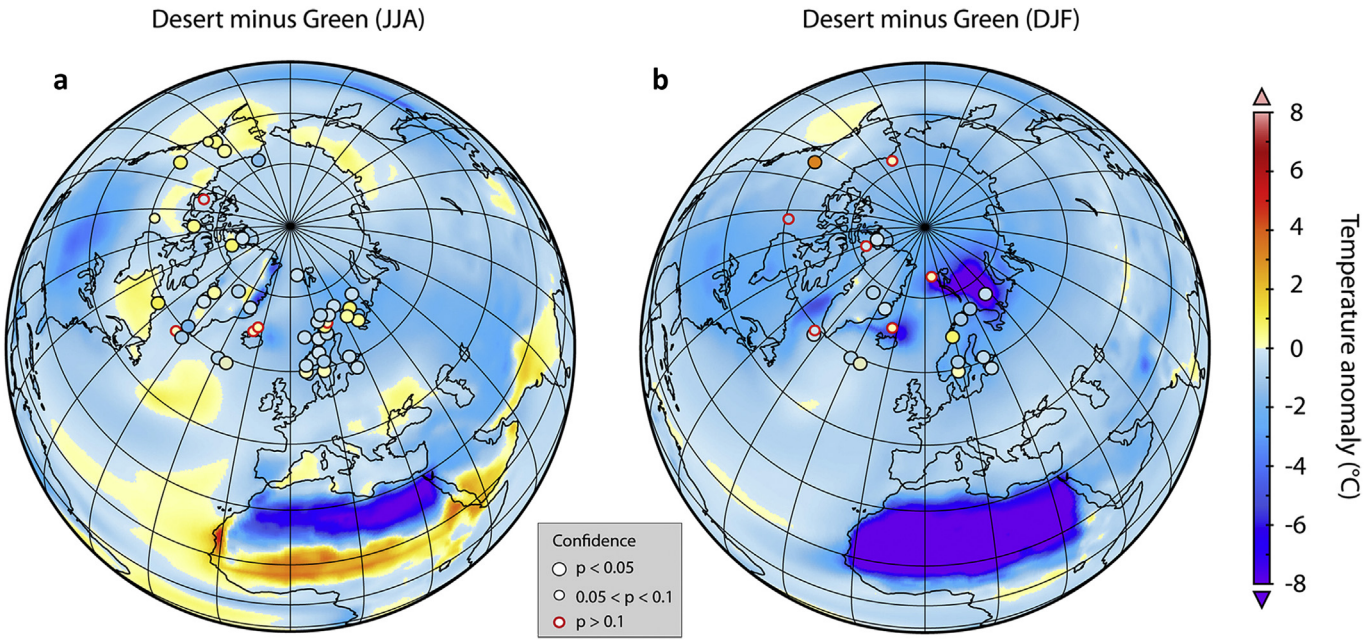

Fig. 1. (**a**) Summer and (**b**) winter distribution of high-latitude surface temperature anomalies (°C) at the transition out of the African Humid Period as inferred from proxy data ($\Delta T_{5kyr-6kyr}$) and EC-Earth simulations (DESERT − GREEN). Temperature anomalies from proxy records were divided according to the seasonal occurrence, whereas mean annual values are overlain in both summer and winter plots. Summer temperature records generally reflect the warmest month (e.g. July over the continent and August over the ocean) and winter temperature records the coldest month (e.g. January over the continent and the ocean). Summer model output refers to JJA and winter output refers to DJF. Summer Level of significance associated with each temperature anomaly is also shown (see Methods). Where locations of proxy data are at short distance from each other the markers representing the proxies are slightly shifted to improve readability.

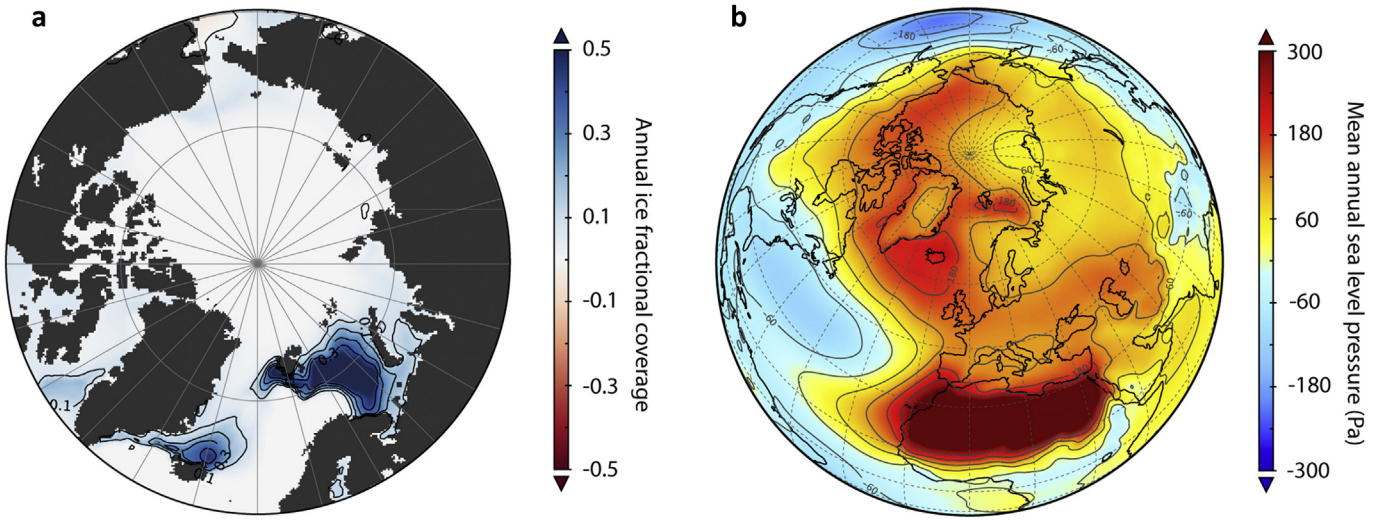

Fig. 2. (**a**) Modelled mean annual sea-ice coverage anomalies and (**b**) mean annual sea-level pressure anomalies (Pa) for DESERT minus GREEN experiments.

between the mid-Holocene climate change and shifts in Saharan vegetation cover existed.

One of the most striking features of the climate shift that stems from our simulations is the large-scale change in SLPs, which resembles a transition from positive Arctic Oscillation (AO+) to negative Arctic Oscillation (AO−) conditions (Fig. 2b). The modern AO− corresponds to cooling and high pressure over the Arctic and Eurasian sectors, and feeble Westerlies across the North Atlantic in response to a switch towards a meridional flow regime (Rigor et al., 2002). The AO− phases are also associated with a weakening of the North Atlantic circulation, with a weakening of wind-driven AMOC and a net decrease in the oceanic heat transport from the subtropics to the northern North Atlantic (e.g. Curry and McCartney, 2001). The weakened oceanic circulation is generally accompanied by increased southward routing of sea ice through the East Greenland Current (Dickson et al., 1996). These features are in line with shifts and patterns in SLP, temperature, atmospheric-ocean circulation and northward heat transport generated by our model simulations.

More interestingly, some of these signatures are fairly well documented in a variety of climate reconstructions at the time of the mid-Holocene climate change. In addition to the generally colder climate conditions at high northern latitudes observed in our network of reconstructions, the interpretation of a change in

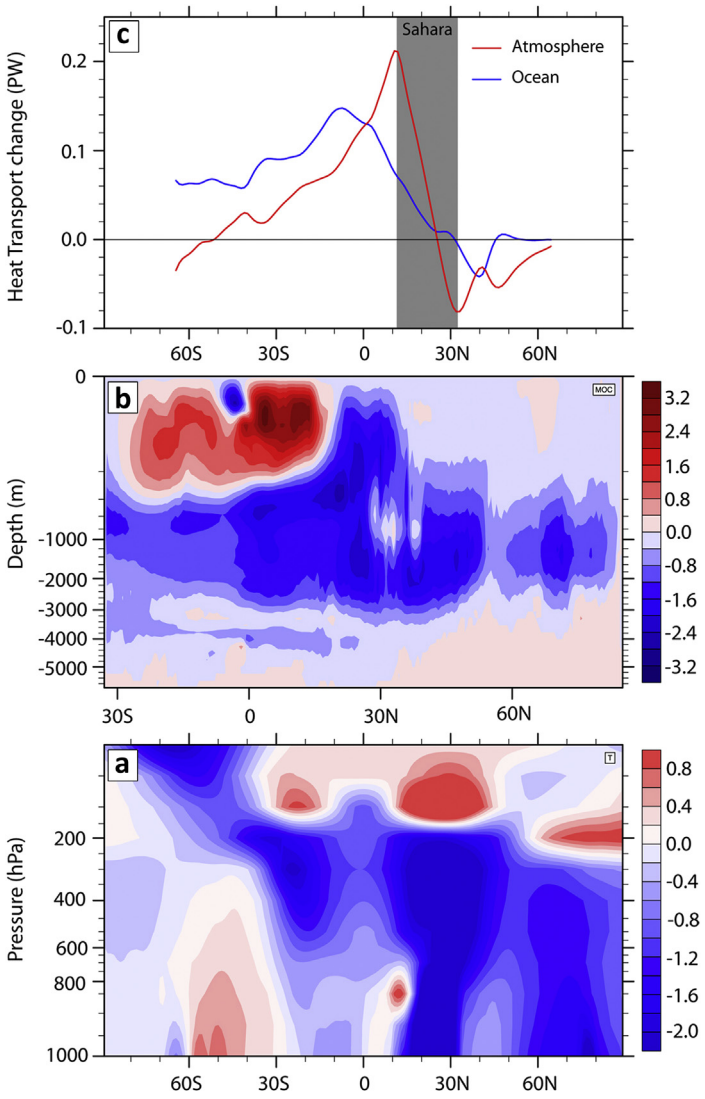

Fig. 3. (**a**) Changes in annual mean vertical temperature averaged over the Atlantic (60W–30E). (**b**) Changes in annual mean Atlantic meridional ocean circulation (Sverdrup). (**c**) Changes in annual mean northward atmospheric and ocean meridional heat transport (PW) over the Atlantic. The latitudinal extent of the Sahara is highlighted for reference. All the changes refer to DESERT minus GREEN results.

circulation regime from AO+ to AO– at 5.5–5.0 kyr BP is also supported by a number of other proxy records. For instance, hydrological reconstructions from northern Europe indicate a marked strengthening of polar anticyclones and increased frequency of cold air outbreaks towards Eurasia at this time (Muschitiello et al., 2013) – a distinctive feature of the AO– (Stein et al., 2004). On the other hand, records from the Arctic Ocean, Northern America, and Greenland point at a major shift towards enhanced meridional flow across the Arctic and the North Atlantic domain (Darby et al., 2001; Kirby et al., 2002; Frechette and deVernal, 2009). Analogously, marine records from the North Atlantic show a concomitant weakening of the ocean circulation (McManus et al., 2004; Kim et al., 2007) accompanied by a transition into a persistent state of weak subpolar gyre circulation (Colin et al., 2010). Finally, marine reconstructions from the northern North Atlantic evidence a rapid transition towards increased sea-ice advection from the Nordic Seas into the East Greenland Current at 5.5–5.0 kyr BP (Jennings et al., 2002).

A further distinctive characteristic correlative to the 5.5–5.0 kyr BP event, which is worth to note, is probably the development of wetter climate conditions in various European regions (Hughes et al., 2000; Magny, 2004; Magny and Haas, 2004; Litt et al., 2009; Kylander et al., 2013). A close correspondence between increased storminess in Europe and augmented export of sea ice southwards from the Nordic Seas to the North Atlantic has been invoked to explain Holocene cool events. Climate simulations (Raible et al., 2007) suggest, for example, that at times of southward advance of the polar front – mediated by export of sea ice to the subpolar North Atlantic – cyclonic activity reinforces south of 50°N in response to steeper meridional oceanic thermal gradients across the North Atlantic.

4. Conclusions

Altogether, the ensemble of regional paleoclimate information deployed here are consistent, at least qualitatively, with the large-scale atmospheric-ocean circulation changes forced by a collapse of Saharan vegetation at the end of the AHP. Using a general circulation model, we demonstrated that the dynamical aspects of the subtropical teleconnective mechanism, in which changes in

Saharan land cover modulate atmospheric and ocean circulation dynamics at high latitudes, is robust. These results also confirm previous outcomes generated with a climate model of intermediate complexity (Davies et al., 2015).

To summarize, the observed physical coupling that links the low and the high latitude climate subsystems implies that interglacial climate is sensitive to land cover changes in the Sahara, with potential implications extending to past interglacial climate scenarios. The impact of changes in albedo brought by environmental shifts in northern Africa on the Earth's climate system carries special significance with respect to the Arctic domain, especially in the debate of high-latitude climate sensitivity and polar climate amplification. Although the actual extent and magnitude of the vegetation collapse in North Africa still remains an open question, our insights help disentangle the complexity of the mid-Holocene climate change and improve the understanding of the spatial pattern of climate shifts associated with this enigmatic period. Future research efforts must supply an adequate spatial characterization of North African vegetation-cover changes across the termination of the AHP. This may help greatly to improve the design of these model experiments and to tackle important questions on the response and sensitivity of polar and subpolar climates to changes in vegetation and land-use types at tropical and subtropical latitudes.

Acknowledgements

F.M., Q.Z., and H.S.S. are supported by the Bolin Centre for Climate Research. The climate model simulations were performed on resources provided by the Swedish National Infrastructure for Computing (SNIC) at NSC and Cray XC30 HPC systems at ECMWF. F.J.D. and H.R. are supported by the 'European Communities 7th Framework Programme FP7/2013, Marie Curie Actions, under grant agreement No. 23811: CASEITN. We thank R. Graham for his helpful comments on this manuscript.

Appendix A. Supplementary data

Supplementary data related to this article can be found at http://dx.doi.org/10.1016/j.quascirev.2015.08.012.

References

Armitage, S.J., Bristow, C.S., Drake, N.A., 2015. West African monsoon dynamics inferred from abrupt fluctuations of Lake Mega-Chad. Proc. Natl. Acad. Sci. 112, 8543–8548.
Arzel, O., Fichefet, T., Goosse, H., 2005. Sea ice evolution over the 20th and 21st centuries as simulated by current AOGCMs. Ocean. Model. 12, 401–415.
Berger, A., 1978. Long-term variations of daily insolation and quaternary climatic changes. J. Atmos. Sci. 35, 2362–2367.
Bond, G., Kromer, B., Beer, J., Muscheler, R., Evans, M.N., Showers, W., Hoffmann, S., Lotti-Bond, R., Hajdas, I., Bonani, G., 2001. Persistent solar influence on North Atlantic climate during the Holocene. Science 294, 2130–2136.
Bosmans, J., Drijfhout, S., Tuenter, E., Lourens, L., Hilgen, F., Weber, S., 2011. Monsoonal response to mid-holocene orbital forcing in a high resolution GCM. Clim. Past Discuss. 7, 3609–3652.
Bouillon, S., Morales Maqueda, M.Á., Legat, V., Fichefet, T., 2009. An elastic–viscous–plastic sea ice model formulated on Arakawa B and C grids. Ocean. Model. 27, 174–184.
Chapman, W.L., Walsh, J.E., 2007. Simulations of arctic temperature and pressure by global coupled models. J. Clim. 20, 609–632.
Claussen, M., Kubatzki, C., Brovkin, V., Ganopolski, A., Hoelzmann, P., Pachur, H.-J., 1999. Simulation of an abrupt change in Saharan vegetation in the mid-Holocene. Geophys. Res. Lett. 26, 2037–2040.
Colin, C., Frank, N., Copard, K., Douville, E., 2010. Neodymium isotopic composition of deep-sea corals from the NE Atlantic: implications for past hydrological changes during the Holocene. Quat. Sci. Rev. 29, 2509–2517.
Curry, R.G., McCartney, M.S., 2001. Ocean gyre circulation changes associated with the North Atlantic oscillation. J. Phys. Oceanogr. 31, 3374–3400.
Darby, D., Bischof, J., Cutter, G., de Vernal, A., Hillaire-Marcel, C., Dwyer, G., McManus, J., Osterman, L., Polyak, L., Poore, R., 2001. New record shows pronounced changes in Arctic Ocean circulation and climate. EOS Trans. Am. Geophys. Union 82, 601–607.
Davies, F.J., Renssen, H., Blaschek, M., Muschitiello, F., 2015. The impact of Sahara desertification on Arctic cooling during the Holocene. Clim. Past 11, 571–586.
Debret, M., Sebag, D., Crosta, X., Massei, N., Petit, J.R., Chapron, E., Bout-Roumazeilles, V., 2009. Evidence from wavelet analysis for a mid-Holocene transition in global climate forcing. Quat. Sci. Rev. 28, 2675–2688.
deMenocal, P., Ortiz, J., Guilderson, T., Adkins, J., Sarnthein, M., Baker, L., Yarusinsky, M., 2000. Abrupt onset and termination of the African Humid Period: rapid climate responses to gradual insolation forcing. Quat. Sci. Rev. 19, 347–361.
Dickson, R., Lazier, J., Meincke, J., Rhines, P., Swift, J., 1996. Long-term coordinated changes in the convective activity of the North Atlantic. Prog. Oceanogr. 38, 241–295.
Fréchette, B., de Vernal, A., 2009. Relationship between Holocene climate variations over southern Greenland and eastern Baffin Island and synoptic circulation pattern. Clim. Past 5, 347–359.
Garcin, Y., Schwab, V.F., Gleixner, G., Kahmen, A., Todou, G., Séné, O., Onana, J.-M., Achoundong, G., Sachse, D., 2012. Hydrogen isotope ratios of lacustrine sedimentary n-alkanes as proxies of tropical African hydrology: insights from a calibration transect across Cameroon. Geochimica et Cosmochimica Acta 79, 106–126.
Gasse, F., 2001. Hydrological changes in Africa. Science 292, 2259–2260.
Gibson, K.A., Peterson, L.C., 2014. A 0.6 million year record of millennial-scale climate variability in the tropics. Geophys. Res. Lett. 41, 969–975.
Hazeleger, W., Severijns, C., Semmler, T., Stefanescu, S., Yang, S., Wang, X., Wyser, K., Dutra, E., Baldasano, J.M., Bintanja, R., 2010. EC-earth: a seamless earth-system prediction approach in action. Bull. Am. Meteorol. Soc. 91, 1357–1363.
Hughes, P.D.M., Mauquoy, D., Barber, K.E., Langdon, P.G., 2000. Mire-development pathways and palaeoclimatic records from a full Holocene peat archive at Walton Moss, Cumbria, England. Holocene 10, 465–479.
Jennings, A.E., Knudsen, K.L., Hald, M., Hansen, C.V., Andrews, J.T., 2002. A mid-Holocene shift in Arctic sea-ice variability on the East Greenland Shelf. Holocene 12, 49–58.
Kim, J.H., Meggers, H., Rimbu, N., Lohmann, G., Freudenthal, T., Muller, P.J., Schneider, R.R., 2007. Impacts of the North Atlantic gyre circulation on Holocene climate off northwest Africa. Geology 35, 387–390.
Kirby, M.E., Mullins, H.T., Patterson, W.P., Burnett, A.W., 2002. Late glacial–Holocene atmospheric circulation and precipitation in the northeast United States inferred from modern calibrated stable oxygen and carbon isotopes. Geol. Soc. Am. Bull. 114, 1326–1340.
Koenigk, T., Brodeau, L., Graversen, R.G., Karlsson, J., Svensson, G., Tjernström, M., Willén, U., Wyser, K., 2013. Arctic climate change in 21st century CMIP5 simulations with EC-Earth. Clim. Dyn. 40, 2719–2743.
Kruschke, J.K., 2013. Bayesian estimation supersedes the *t* test. J. Exp. Psychol. General 142, 573.
Kuhlmann, H., Meggers, H., Freudenthal, T., Wefer, G., 2004. The transition of the monsoonal and the N Atlantic climate system off NW Africa during the Holocene. Geophys. Res. Lett. 31, 22.
Kuper, R., Kröpelin, S., 2006. Climate-controlled Holocene occupation in the Sahara: motor of Africa's evolution. Science 313, 803–807.
Kylander, M.E., Bindler, R., Cortizas, A.M., Gallagher, K., Mörth, C.-M., Rauch, S., 2013. A novel geochemical approach to paleorecords of dust deposition and effective humidity: 8500 years of peat accumulation at Store Mosse (the "Great Bog"), Sweden. Quat. Sci. Rev. 69, 69–82.
Litt, T., Schoelzel, C., Kuehl, N., Brauer, A., 2009. Vegetation and climate history in the Westeifel Volcanic Field (Germany) during the past 11,000 years based on annually laminated lacustrine maar sediments. Boreas 38, 679–690.
Liu, Z., Wang, Y., Gallimore, R., Notaro, M., Prentice, I.C., 2006. On the cause of abrupt vegetation collapse in North Africa during the Holocene: climate variability vs. vegetation feedback. Geophys. Res. Lett. 33, 22.
Madec, G., 2008. NEMO Ocean Engine, Note du Pole de Modlisation. Institut Pierre-Simon Laplace (IPSL), Paris, France. No. 27, ISSN No. 1288–1618.
Magny, M., 2004. Holocene climate variability as reflected by mid-European lake-level fluctuations and its probable impact on prehistoric human settlements. Quat. Int. 113, 65–79.
Magny, M., Haas, J.N., 2004. A major widespread climatic change around 5300 cal. yr BP at the time of the Alpine Iceman. J. Quat. Sci. 19, 423–430.
Manning, K., Timpson, A., 2014. The demographic response to Holocene climate change in the Sahara. Quat. Sci. Rev. 101, 28–35.
McGee, D., deMenocal, P., Winckler, G., Stuut, J., Bradtmiller, L., 2013. The magnitude, timing and abruptness of changes in North African dust deposition over the last 20,000 yr. Earth Planet. Sci. Lett. 371, 163–176.
McManus, J., Francois, R., Gherardi, J.-M., Keigwin, L., Brown-Leger, S., 2004. Collapse and rapid resumption of Atlantic meridional circulation linked to deglacial climate changes. Nature 428, 834–837.
Muschitiello, F., Schwark, L., Wohlfarth, B., Sturm, C., Hammarlund, D., 2013. New evidence of Holocene atmospheric circulation dynamics based on lake sediments from southern Sweden: a link to the Siberian High. Quat. Sci. Rev. 77, 113–124.
Patricola, C.M., Cook, K.H., 2008. Atmosphere/vegetation feedbacks: a mechanism for abrupt climate change over northern Africa. J. Geophys. Res. Atmos. 113, D18102.
Raible, C.C., Yoshimori, M., Stocker, T.F., Casty, C., 2007. Extreme midlatitude cyclones and their implications for precipitation and wind speed extremes in

simulations of the Maunder Minimum versus present day conditions. Clim. Dyn. 28, 409–423.
Rigor, I.G., Wallace, J.M., Colony, R.L., 2002. Response of sea ice to the Arctic oscillation. J. Clim. 15, 2648–2663.
Shanahan, T.M., McKay, N.P., Hughen, K.A., Overpeck, J.T., Otto-Bliesner, B., Heil, C.W., King, J., Scholz, C.A., Peck, J., 2015. The time-transgressive termination of the African Humid Period. Nat. Geosci. 1, 1–5.
Sorrel, P., Debret, M., Billeaud, I., Jaccard, S.L., McManus, J.F., Tessier, B., 2012. Persistent non-solar forcing of Holocene storm dynamics in coastal sedimentary archives. Nat. Geosci. 5, 892–896.
Stein, R., Dittmers, K., Fahl, K., Kraus, M., Matthiessen, J., Niessen, F., Pirrung, M., Polyakova, Y., Schoster, F., Steinke, T., Futterer, D.K., 2004. Arctic (palaeo) river discharge and environmental change: evidence from the Holocene Kara Sea sedimentary record. Quat. Sci. Rev. 23, 1485–1511.
Sundqvist, H., Kaufman, D., McKay, N., Balascio, N., Briner, J., Cwynar, L., Sejrup, H., Seppä, H., Subetto, D., Andrews, J., 2014. Arctic Holocene proxy climate database–new approaches to assessing geochronological accuracy and encoding climate variables. Clim. Past Discuss. 10, 1–63.
Tierney, J., deMenocal, P., 2013. Abrupt shifts in Horn of Africa hydroclimate since the Last Glacial Maximum. Science 342, 843–846.
Valcke, S., 2006. OASIS3 User Guide (Prism_2–5). PRISM support initiative report 3, p. 64.
Wirtz, K.W., Lohmann, G., Bernhardt, K., Lemmen, C., 2010. Mid-Holocene regional reorganization of climate variability: analyses of proxy data in the frequency domain. Palaeogeogr. Palaeoclimatol. Palaeoecol. 298, 189–200.
Zhao, Y., Braconnot, P., Harrison, S., Yiou, P., Marti, O., 2007. Simulated changes in the relationship between tropical ocean temperatures and the western African monsoon during the mid-Holocene. Clim. Dyn. 28, 533–551.